Examination of EMC Chamber Qualification Methodology for Applications above 1 GHz Using Frequency Domain Mode Filtering

Zhong Chen
ETS-Lindgren
1301 Arrow Point Drive, Cedar Park, TX, USA
zhong.chen@ets-lindgren.com

Stuart Gregson
Next Phase Measurements
11521 Monarch St, Garden Grove, CA, USA
stuart.gregson@npmeas.com

***Abstract*—Anechoic chambers used for Electromagnetic Compatibility (EMC) measurements above 1 GHz are qualified based on the Site Voltage Standing Wave Ratio (SVSWR) method as per the international standard CISPR 16-1-4. The SVSWR measurements consist of a series of scalar measurements using a dipole-like antenna placed along several linear transmission paths that are located at the edge of the quiet zone (QZ). Another antenna is placed at a fixed position in the chamber pointing towards the center of the QZ. The measurement process is conceptually similar to measuring VSWR using a slotted line and a moving probe. A full set of tests is time consuming because of the number of positions, antenna heights, polarizations and frequencies that are generally required. To reduce the test burden, the SVSWR method "intentionally" under-samples the measurement by requiring only 6 measurement points along each 40 cm long linear path to characterize the standing wave. As a result, the test results are generally overly optimistic. At microwave frequencies (note the upper frequency limit is 18 GHz), this under-sampling becomes far more pronounced. In this paper, we explore the effectiveness of using Cylindrical Mode Coefficient (CMC) based frequency domain mode filtering techniques to obtain the VSWR, essentially applying the mode filtering algorithm to separate the antenna response from the chamber reflections. Here, we place the dipole-like test antenna on the outer edge of the turntable to obtain a full rotational pattern cut of amplitude and phase data. The antenna is then mathematically translated to the rotation center, whereupon a band-pass filter that tightly encloses the test antenna mode spectrum is applied. The difference between the mode filtered antenna pattern and the original perturbed pattern is attributed to chamber reflections. The measurement is comparatively easy to implement with no special positioning equipment needed although phase information is required. However, this is readily available in most modern test setups. In this paper we present measured results taken from two horizontal polarization measurements (where the antennas were oriented 90 degrees from each other), and one vertical polarization measurement. For an EMC chamber test at a fixed height, an entire measurement campaign reduces to taking three vector pattern cuts. In contrast to the conventional technique, the proposed, novel, method does not suffer from positional under-sampling, so it is well-placed to be applied at microwave frequencies and above.**

Index Terms—EMC, SVSWR, Mode Filtering, Cylindrical Mode Coefficient.

I. Introduction

Site Voltage Standing Wave Ratio (SVSWR) is used as a metric to qualify the performance of anechoic chambers used for Electromagnetic Compatibility (EMC) testing at frequencies above 1 GHz [1]. A typical test configuration is shown in Fig. 1. A dipole-like omni-directional antenna is placed at various locations in the Quiet Zone (QZ), such as at the Front (F), Left (L), or Right (R) locations. The other antenna, which is typically a broadband ridged waveguide horn, is located some distance away (usually 3 m) and is boresighted to the center of the QZ. The omni-directional antenna is used to sample the standing wave along several 40 cm linear paths, each consisting of six discrete positions (at 0 cm, 2 cm, 10 cm, 18 cm, 30 cm, and 40 cm away from the first position). As is well documented [2], the six discrete positions are chosen as a compromise to save test time. These irregularly spaced positions are attempts at breaking up possible harmonics. Nonetheless, they severely under-sample the standing wave, and the resulting VSWR is characteristically less stringent.

In [3], an alternative technique is proposed by performing several single pattern cut measurements with the omni-directional antenna set at the edge of the QZ. The resulting pattern is then compared with numerical simulations reconstructed from the antenna's Spherical Mode Coefficients (SMC) to derive the SVSWR ripple size. The difference in dB between the raw pattern to the reference data is the chamber SVSWR. The method is attractive in that the setup and measurement processes are rather simple. The antenna is rotated by the turntable, which is readily available in any EMC chamber. There is no need to under-sample the antenna pattern by taking a sparse angular step, as the measurement can be

easily automated. However, one drawback is that the results and accuracy depend on a priori knowledge of the antenna pattern. This could be onerous due to the fact that the antenna must be numerically modelled or calibrated beforehand which increases the burden on the experimentalist.

In this study, we take a different approach to obtain the reference antenna pattern by applying the far-field cylindrical mode filtering technique [4, 5]. In [5], it has been shown that this is an effective measurement and post processing technique that can be used to correct far-field antenna pattern data where only a single polarized great circle pattern cut is taken. Because the antenna is offset from the center of the measurement coordinate system, which in this case is the rotation axis of the azimuth stage, mode orthogonalization and filtering is a natural candidate to remove the chamber reflections and to obtain the reference pattern. No a priori knowledge of the antenna pattern, auxiliary measurements, or Computational Electromagnetic (CEM) simulations is needed. The SVSWR measurement process thus reduced to performing several one-dimensional pattern cuts. As is proposed in [3], we collect three pattern cuts, *i.e.*, one with antennas vertical polarized, two with antenna horizontal polarized, but are oriented 90° from each other (either parallel with *x*- or *z*-axes at F6 as is illustrated in Fig. 1).

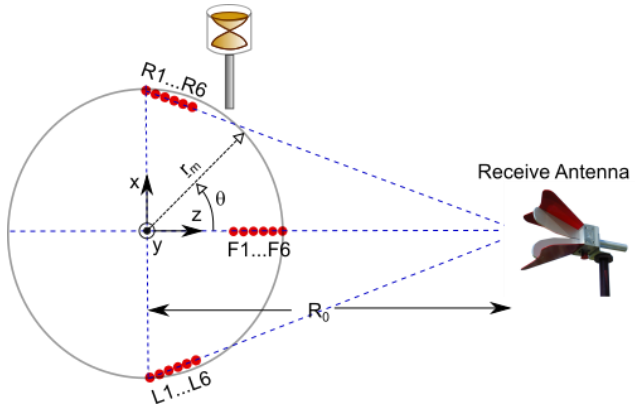

Fig. 1. SVSWR test setup per CISPR 16-1-4.

Fig. 2 and Fig 3 shows different views of the test setup showing the offset biconical test antenna in the test chamber.

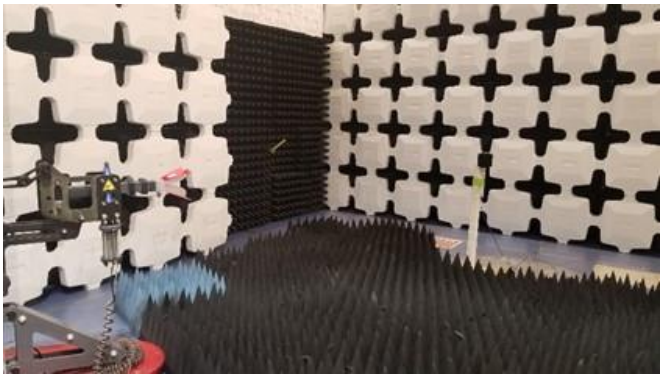

Fig. 2. Test setup showing EMC chamber with the remote source antenna seen to the left and the biconical to the right.

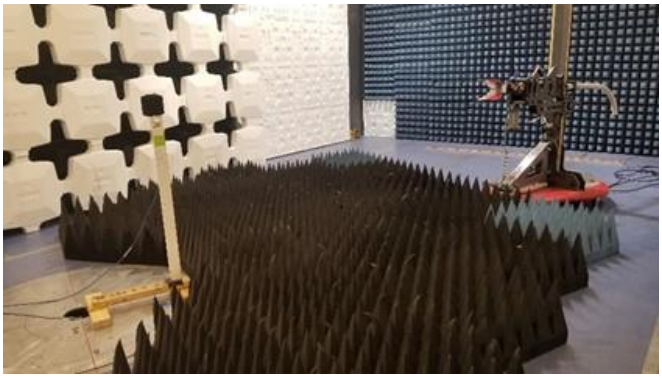

Fig. 3. Opposite view of test setup showing the offset biconical.

Here, the receive antenna was an ETS-Lindgren Model 3117 double-ridged waveguide horn whilst the test antenna was an ETS-Lindgren Model 3183B end-fed mini-biconical antenna. Both instruments operate from 1 to 18 GHz. The mini-biconical test antenna is specifically designed to meet the pattern requirements in CISPR 16-1-4 and ANSI C63.25.1 [6] for chamber validation testing.

II. Theoretical Background and Development

A detailed development of mode filtering-based scattering suppression measurement and post-processing-based techniques is beyond the scope of this paper and is instead left to the open literature, *e.g.* [5], with merely a summary being presented herein. An antenna is generally installed within a test range in such a way that it is displaced as little as possible during an acquisition. Range multi-path reflections disturb the fields illuminating the AUT, thus the purpose of this strategy is to guarantee the illuminating field changes minimally during the acquisition, and in so doing minimizing any resulting measurement error. However, this measurement technique intentionally displaces the AUT away from the center of rotation [4, 5]. This significantly increases the differences in the illuminating field making range multipath effects far more pronounced than they would otherwise. It is exactly this greater differentiation that makes the identification and extraction of range multipath viable.

Clearly, displacing the AUT from the center of rotation will increase the effective electrical size of the AUT. From standard cylindrical near-field theory we may calculate the angular sample spacing using [5],

$$\Delta\theta = \frac{2\pi}{2\left(\mathrm{ceil}\left(k_0\rho_0\right)+n_1\right)+1} \tag{1}$$

Here, ***ceil*** is used to denote a function that rounds to the nearest integer towards positive infinity, n_1 is a positive integer that depends upon the accuracy required (*e.g.* $n_1 = 10$ [5]), k_0 is the free-space wave number, and ρ_0 is the maximum radial extent which is a cylinder that is coaxial with the azimuth axis and that is large enough to circumscribe the majority of the current sources [5]. However, as only a single cut is required, the additional data will not typically affect the duration of the measurement providing the measurements are taken on-the-fly and the receiver is sufficiently fast to be able to acquire the data before the next sample point is encountered.

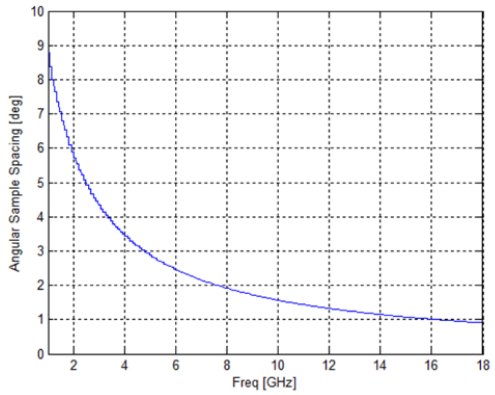

Fig. 4. Sample Spacing plotted as a function of frequency for a 0.5 m MRE measurement.

This is illustrated below for the case of a measurement with a 0.5 m Maximum Radial Extent (MRE) confirming that a 1° angular sample spacing is easily sufficient for measurements to 16 GHz and approximately sufficient for measurements to 18 GHz as a result of the asymptotic nature of the curve and inclusion of the safety factor n_1. For a multi-frequency measurement, this would be satisfied for the highest frequency.

Traditionally, translating the test antenna in this way also has an impact on the far-field distance [5] as this can be expressed in terms of the MRE. Thus conventionally, increasing the MRE will similarly increase the required range length such that,

$$R = \frac{2D^2}{\lambda} \approx \frac{2(2\rho_0)^2}{\lambda} = \frac{8\rho_0^2}{\lambda} \tag{2}$$

However, as we shall consider below, with the use of an appropriate translation operator this is perhaps an overly conservative criteria for our particular application. Once a far-field cut has been taken, the AUT must be translated to the origin of the measurement coordinate system. In the true far-field this is achieved by purely adjusting the phase, see [4, 5],

$$\underline{E}_t(r \to \infty, \theta) = \underline{E}(r \to \infty, \theta) e^{jk_0 \cdot \underline{r}_m} \tag{3}$$

Here, $\underline{r}_m$ is used to denote the displacement vector between the center of the measurement coordinate system and the center of the current sources. In the true far-field this expression is exact, however in the case where the measurement range length is large but not infinitely large, a better correction can be obtained by incorporating the change in the finite range length making the amplitude and phase translation correction,

$$\underline{E}_t(\theta) = \underline{E}(\theta) e^{jk_0\left(\sqrt{\left(R_0 - |\underline{r}_m|\cos\theta\right)^2 + \left(|\underline{r}_m|\sin\theta\right)^2} - R_0\right)} \times \frac{\sqrt{\left(R_0 - |\underline{r}_m|\cos\theta\right)^2 + \left(|\underline{r}_m|\sin\theta\right)^2}}{R_0} \tag{4}$$

Here, R_0 denotes the distance between the Remote Source Antenna (RSA) and the center of the azimuth rotation stage, which is serving as the origin of the measurement coordinate system and the symbol × denotes scalar multiplication, and *not* the vector cross-product. For a typical measurement, this correction is on the order of one or two dB. However, when using a vertically polarized bi-conical as the test antenna the effect of the correction is evident and can be seen illustrated in Figs. 5 and 6 below.

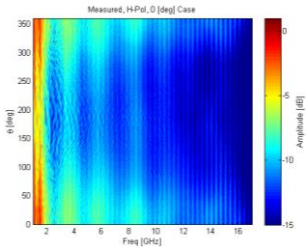

Fig. 5. Measured quasi far-field pattern data plotted as a false color plot over frequency.

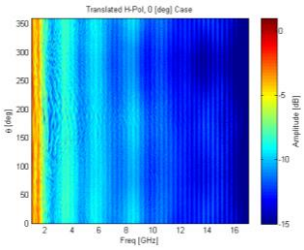

Fig. 6. Translated quasi far-field pattern data plotted as a false color plot over frequency.

This mathematical translation has the effect of reducing the number of mode coefficients, spherical or cylindrical *etc*., that are required to describe the equivalent far-field pattern [4, 5]. This is important since, by (2) as viewed traditionally, we are not in the true far-field. However, the data that we supply to the mode processing has been translated to the origin, using (4) and thus to a first order, with the finite range length amplitude and phase corrections applied, the mode processing is utilizing to a good approximation reliable far-field data. Thus, the traditional application of the far-field criteria may consider the conceptual minimum MRE of the AUT in the calculation of the far-field distance as opposed to using the conventional MRE. However, it is important to recognize that the translation operator is approximate in general and valid for electrically small antennas only. For example, it is rigorous for an infinitesimal dipole, but becomes progressively more unreliable as the electrical size of the test antenna increases for a given fixed, finitely large range length. Crucially however, the test antenna that is employed within this testing regime is by design an electrically small, low directive antenna making it a very viable candidate for this approach.

The equivalent Cylindrical Mode Coefficients (CMCs) can be obtained from the compensated far-electric-fields using standard cylindrical theory [5],

$$B_n^1(\gamma) = -\frac{(-j)^{-n}}{4\pi} \int_0^{2\pi} E_\theta(r \to \infty, \theta) e^{-jn\theta} d\theta \tag{5}$$

$$B_n^2(\gamma) = -\frac{(-j)^{-n}}{4\pi} \int_0^{2\pi} E_\phi(r \to \infty, \theta) e^{-jn\theta} d\theta \tag{6}$$

Here, θ represents a rotation about the vertical azimuthal axis (this is a more convenient coordinate system for our application; however, it does differ from what is commonly used in the development of the standard cylindrical near-field theory). For a fixed measurement radius and frequency, these B_n mode coefficients are complex numbers that do not vary with any of the scanning variables and conversely are functions of n the angular index, and γ the Fourier variable such that $-\infty \le n \le \infty$ and $-\infty \le \gamma \le \infty$. Here, as per the usual convention, the unimportant far-field spherical phase factor and inverse r term have been suppressed.

A comparison of the equivalent CMCs for the case where the test antenna has been translated to the origin using the asymptotic far-field translation (3) and the modified quasi-far-field translation (4) can be seen in Fig. 7 where the axes have been adjusted to emphasize the AUT modes. From inspection of Fig. 7, it is evident that the CMCs are far more narrowly distributed about the 0th order mode for the case where the more accurate quasi far-field translation operator has been used than is the case for the ideal far-field translation. This results in a far more effective filtering of the CMC spectra providing a more reliable chamber performance estimation that would otherwise be the case. It is worth noting that this operator is not limited to the EMC application being considered here but rather can be used with any far-field measurement, excluding of course measurement where the data was acquired using a Compact Antenna Test Range (CATR). Here, it is worth noting that these transforms and their inverse operations can be evaluated using the one-dimensional fast Fourier transform (FFT) which makes the processing algorithm very efficient in terms of computational effort. It is however worthwhile to use a mixed radix FFT so as to be able to work with arrays which are not a power of two long so as to be able to not zero-pad the data and therefore preserve the accuracy of the reconstructed mode-filtered far-field pattern cut at the edges of the sampling interval.

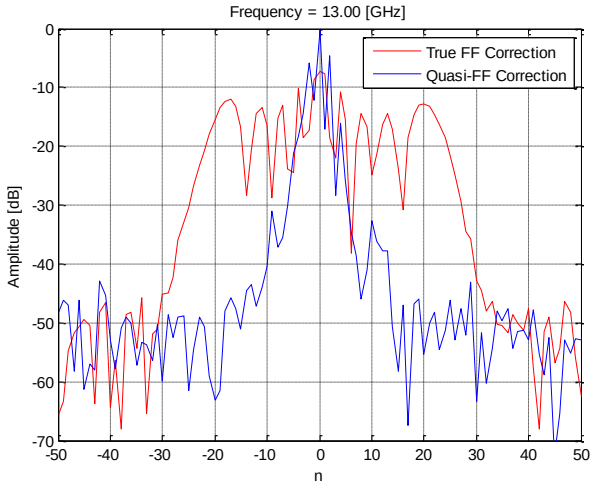

Fig. 7. Comparison of CMC spectra following antenna translation using true far-field correction, red, and quasi far-field correction blue.

Strictly, equations (5) and (6) are only valid in the true far-field. However, providing the measurements are taken with a finite but sufficiently large range length that guarantees the far-field condition is satisfied [5], these integrals may be used with a high degree of confidence. Equally, probe pattern correction can be ignored since in the far-field the MRE cylinder only subtends a very small angular region as observed from the RSA [5]. That is, RSA pattern is sufficiently constant across the test antenna. Lastly, the highest order cylindrical mode that can be calculated from the far-field measured data is determined from [5],

$$n_{\mathrm{Max}} = \mathrm{ceil}\left(\frac{\pi}{|\Delta\phi|}\right) \tag{3}$$

From inspection of (5) & (6), the transverse electric (TE) and transverse magnetic (TM) CMCs are uncoupled from one another and that the θ- and ϕ-polarized electric fields are also uncoupled from one another. This therefore allows this processing to be applied to only a *single* far electric field component. Dual polarized acquisitions are therefore not required in all instances offering the possibility of further reducing test times.

When the cylindrical mode coefficients for the now ideally positioned AUT have been recovered, any mode representing fields outside the ideal conceptual minimum MRE (r_t) can be filtered out, removing contributions that are not associated with the AUT [5]. Hence, because of standard cylindrical theory [5], it is possible to remove all higher order modes without degrading the integrity of the underlying antenna pattern. Several different band-pass filter functions may be employed for this task, with a cosine squared windowing function constituting a good candidate [5].

As a full great-circle cut is acquired, in the absence of blockage, this affords the experimentalist the possibility of determining the AUT offset. This can be done either in the time domain by comparing the difference in the time of arrival for the $\theta = 0°$ and $\theta = 180°$ positions, or by examining the phase change between the two positions. In either case, half the difference is the AUT offset radius. In many instances it is easier and more accurate to determine the magnitude of the displacement in this way rather than by attempting to determine it directly, with a tape measure *etc*. In this case, the time difference was 3.23 ns or equivalently 0.969 m therefore making the AUT displacement 0.4845 m.

In effect then, the contributions in the CMC domain of the AUT and the scatterers are separated by the translation so that they do not interfere with one another and are therefore orthogonalized [7]. The inversion of (5) and (6) is then used to reconstruct the filtered far-field pattern [4]. A comparison of the measured, *i.e.* perturbed cut, and the filtered, *i.e.* reference cut, can be used to obtain the ripple in the measurement. The difference between the maximum and minimum ripple as a function of frequency is thus used to characterize the chamber. Results of this processing are presented and discussed in the following section.

III. Experimental Results

The experimental arrangement depicted in Fig. 1. and shown in Fig. 2 and Fig. 3. was used to acquire the amplitude data shown in Fig 5 and accompanying phase data, not shown due to space constraints. The algorithm set out above in Section II was then used to compute the mode filtered great circle far-field pattern cut across the 1 to 18 GHz frequency band with 1601 frequency points. Fig. 8 contains a plot of the equivalent CMC spectrum for the 2 GHz case, which is a frequency that the chamber is known to perform less well due to the transition between the dielectric foams and the ferrite tiles used by the hybrid absorbers. Here, the reconstructed CMCs prior to filtering clearly show the effects of higher order modes that are a consequence of chamber reflections. The CMCs are filtered, using a cosine squared filter function, whereupon the mode

filtered far-field pattern is computed. Fig. 9 contains the equivalent plot showing the measured great circle far-field azimuth pattern cut with and without mode filtering, which are denoted by the blue and black traces, respectively. The magenta trace is the difference plot which permits us to obtain a measure of the performance of the chamber at this specific frequency. In practice this is accomplished by computing the maximum of the difference minus the minimum of the difference. This enables us to determine the SVSWR. Thus, in essence we are looking at the difference between a scattering contaminated antenna measurement and a "clean" antenna measurement. Since the antenna pattern is the same in each case the precise properties of its pattern can be seen to be suppressed when we compute the difference thereby reducing the sensitivity of this technique to the influence of the particular antenna being used, providing of course that the measurement is sufficiently sensitive.

It should be noted, standard deviation of the ripple values can be calculated here, and instead of reporting the maximum difference as the SVSWR, results using a different statistical coverage factor can be reported, similar to the way time domain SVSWR is treated in ANSI C63.25.1 [6] in order to match the test severity of the CISPR SVSWR results.

Similarly, Fig. 10 and Fig. 11 are equivalent plots for the 8 GHz case which is a frequency at which the chamber is known to perform well. The slightly broader AUT spectra is a natural consequence of a fixed MRE and an increase in frequency permitting a larger number of modes to be used to represent the same antenna as from the sampling theorem the maximum mode that is associated with the AUT is $n_{\max} = k_0 a$ where a is the MRE [4]. Thus, at each frequency the mode windowing function is adjusted to take this into account. Here, by comparing the respective magenta traces in Fig. 9 and Fig. 11, we may evaluate the difference in the performance of the anechoic chamber at these two frequencies. Thus, by computing this site VSWR at each frequency it is possible to build up a measure of the chamber's performance across the 1 to 18 GHz band. This can be seen presented in Fig. 12 for the vertical polarization case, and Fig. 13 for one of the horizontal polarization cases. It was also noted the result was relatively insensitive to angular sample spacing with very similar SVSWR results being obtained when only half the number of angular samples were utilized by the processing.

To further validate the proposed method, the result shown in Fig. 12 is compared to the time domain SVSWR (TD SVSWR). The TD SVSWR method is described in ANSI C63.25.1 [6], where time domain gates are applied around the main antenna-to-antenna impulse response. The chamber reflection coefficient ($|\Gamma|$) is calculated by taking the ratio of the band-stop gated frequency response to the band-pass gated data. The SVSWR is then given by,

$$SVSWR = \frac{1+|\Gamma|}{1-|\Gamma|} \tag{8}$$

Fig. 14 shows the TD SVSWR for the F6 position (for the vertical polarization, and at $\theta = 0°$). Considering the TD SVSWR data is for a single test position, whereas Fig. 12 is obtained from the entire circular cut, from inspection it can be seen that these results agree rather well.

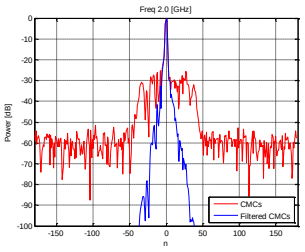

Fig. 8. CMCs plot before and after filtering @ 2 GHz, where the chamber's performance is poorest.

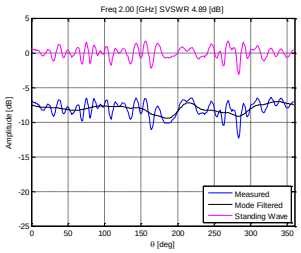

Fig. 9. Azimuth cut with and without processing where the chamber's performance is poorest.

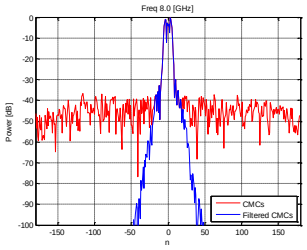

Fig. 10. CMCs plot before and after filtering @ 8 GHz, where the chamber's performance is best.

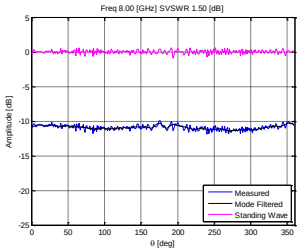

Fig. 11. Azimuth cut with and without processing where the chamber performance is best.

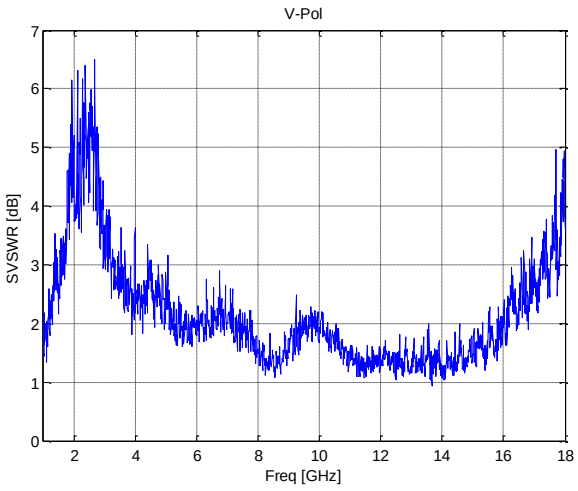

Fig. 12. SVSWR plot for V-pol measurement.

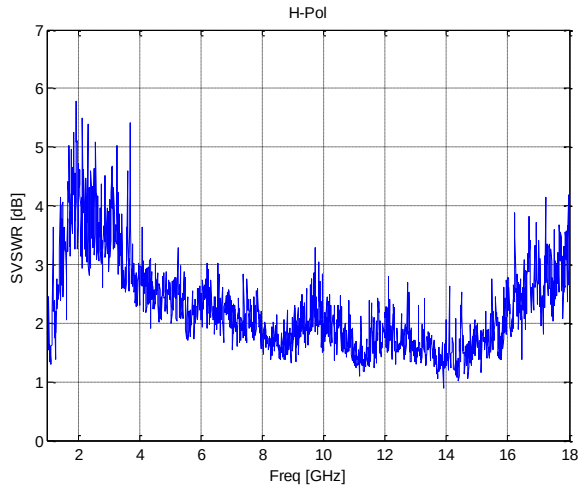

Fig. 13. SVSWR plot for H-pol measurement.

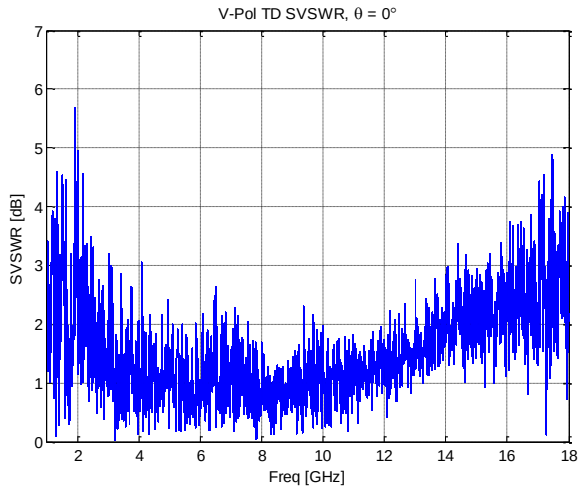

Fig. 14. SVSWR plot for V-pol measurement as computed using the time domain filtering method, *cf.* Fig. 12 above.

IV. Summary and Conclusions

In this study, a novel SVSWR measurement method for evaluating EMC chambers is proposed based on placing an omni-directional antenna at the outer edge of the turntable and collecting vector data for several 1D pattern cuts. Cylindrical Mode Coefficients filtering is applied to separate the antenna response from the chamber reflections based on the cylindrical mode filtering algorithm. The difference between the uncorrected pattern and the mode filtered pattern is used to derive the SVSWR. The proposed method also overcomes the difficulty associated with under-sampling the standing wave pattern in the traditional CISPR SVSWR technique. It is easy to implement using existing turntable in an EMC chamber, with no other special positioning equipment needed. Three great circle pattern cuts with different antenna orientations are proposed, which can fully quantify the chamber SVSWR, therefore the measurement data can be acquired with minimal test time. Compared to the TD SVSWR method specified in the ANSI C63.25.1 standards, the proposed method does not rely on using broadband antennas or antennas with short ring-down times. Unlike the CTIA ripple test, the method also does not rely on a priori knowledge of the antenna patterns, so it could potentially be used as an expedient alternative in those types of applications. Preliminary results show good correlation with the existing SVSWR method. Lastly, a further validation and correlation study is planned which will include amongst other activities, a closer examination of the angular sampling requirements for this new measurement technique.

Acknowledgment

The authors wish to thank David Macklom at ETS-Lindgren for collecting the measurement data.

References

[1] "Specification for radio disturbance and immunity measuring apparatus and methods - Part 1-4: Radio disturbance and immunity measuring apparatus - Antennas and test sites for radiated disturbance measurements," CISPR/CIS/A, CISPR 16-1-4:2019, Jan. 2019.

[2] Z. Chen, "Uncertainties in SVSWR and a proposal for improvement using vector response measurements," 2014 International Symposium on Electromagnetic Compatibility, Tokyo (EMC'14 / Tokyo).

[3] C. Culotta-Lopez, Z. Chen, T. Gemmer, D. Heberling, "Validation of electromagnetic compatibility chambers with a spherical wave expansion approach," in Antenna Measurement Techniques Association Symposium (AMTA), 2019.

[4] S. Gregson, et. al., "Application of Mathematical Absorber Reflection Suppression to direct Far-Field antenna range measurements," in Antenna Measurement Techniques Association Symposium (AMTA), 2011.

[5] C.G. Parini, S.F. Gregson, J. McCormick, D. Janse van Rensburg "Theory and Practice of Modern Antenna Range Measurements", IET Press, 2014, ISBN 978-1-84919-560-7.

[6] ANSI C63.25.1-2018: American National Standard Validation Methods for Radiated Emission Test Sites, 1 GHz to 18 GHz, 2019.

[7] S.F. Gregson, Z. Tian, "Verification of Generalized Far-Field Mode Filtering Based Reflection Suppression Through Computational Electromagnetic Simulation", IEEE International Symposium on Antennas and Propagation and North American Radio Science Meeting, 5-10 July 2020, Montréal, Québec, Canada.